WPMST2-PR(18) 20557

L Piron et al.

Error field control strategies towards MAST Upgrade operation

Preprint of Paper to be submitted for publication in
Nuclear Fusion

This work has been carried out within the framework of the EUROfusion Consortium and has received funding from the Euratom research and training programme 2014-2018 under grant agreement No 633053. The views and opinions expressed herein do not necessarily reflect those of the European Commission.

Error field control strategies towards MAST Upgrade operation

L. Piron[1], A. Kirk[1], Y.Q. Liu[1,2], G. Cunningham[1], M. Carr[1], G. Fishpool[1], R. Gowland[1], I. Katramados[1], D. Luckin[3], R. Martin[1]
[1] *CCFE, Culham Science Centre, Abingdon, OX14 3DB, UK*
[2] *General Atomics, P.O. Box 85608, San Diego, California 92186-5608, USA*
[3] *Tesla Engineering Ltd, Water Lane, Storrington, RH20 3EA, UK*
(Dated: May 11, 2018)

Abstract In magnetic fusion devices, unwanted non-axisymmetric magnetic field perturbations, known as error fields (EF), can have detrimental effects on plasma stability and confinement. To minimize their impact on plasma performances and on the available operational space, it is important to identify the EF sources and develop EF control strategies. MAST Upgrade is a magnetic fusion device which will operate in the next future after a series of enhancements from the previous MAST experiment and will contribute to the mainstream program of the exhaust and fast particle physics *[Morris A. W. et al, "MAST Accomplishments and Upgrade for Fusion Next-Steps" IEEE Transactions on Plasma Science, April 2014].* To deliver a machine with EF amplitude low enough to allow a high quality experimental programme, a careful analysis of the intrinsic EF sources in the poloidal field and in the divertor coils has been carried out. The 3D coil deformation has been characterized through high accuracy magnetic field measurements which reveal that the main EF harmonics have n=1 and n=2 toroidal mode numbers. Passive and active control strategies have been adopted to compensate them in preparation for MAST Upgrade operations. The passive EF control consisted in finding the optimal fine-scale coil alignment so as to minimize the intrinsic n=1 EF amplitude. The optimal coil alignment has been determined based on magnetic field measurements and the corresponding 3D electro-magnetic modelling. Conversely, active control will be adopted during MAST Upgrade operation to reduce the n=2 EF which is associated mainly to the manufacturing of the poloidal field coils named P4 and P5 *[Kirk A. et al 2014 Plasma Phys. Control. Fusion 56 104003].* Since these coils have been re-used from the MAST device, the experience gained on n=2 EF control, from experimental studies and the corresponding ERGOS *[Nardon E. et al 2007 J. Nucl. Mater. 363-365 1071]* and MARS-F *[Liu Y. Q. et al 2000 Phys. Plasmas 7 3681]* modelling, has allowed the identification of the best n=2 EF control technique and to perform a model-based optimization of its control parameters in preparation to MAST Upgrade operation.

I. INTRODUCTION

In magnetic fusion devices, unwanted non-axisymmetric magnetic field perturbations, known in literature as error fields (EFs), can arise due to imperfections or misalignment of the coils, because of coil current feeds, eddy currents associated with 3D wall structures and ferritic material in the vicinity of the plasma. In particular, EFs with amplitude δB as small as $\delta B/B_t \approx 10^{-4}$ (where B_t is the toroidal magnetic field) can have a large impact on energy confinement and plasma stability [1–6]. For example, components of these EFs can resonate at low order rational surfaces, i.e. safety factor, q = 1, 2, 3, driving tearing instabilities. This process can induce a braking of the plasma rotation if the EFs have a sufficient amplitude to overcome plasma shielding effects [7, 8]. EFs can also have detrimental effects on plasma performance by damping plasma rotation through the neoclassical toroidal viscosity (NTV) [9–12], by inducing fast particle losses [13, 14] and by triggering ideal-MHD instabilities when exploring high-β regimes [15, 16].

For these reasons, the impact of EFs on plasma performance has long been known to pose a concern in present fusion experiments and to the operation of ITER. Indeed low-n EFs are a significant problem for ITER, in particular in view of potential danger of mode locking during the plasma start-up phase, where significant amount of EFs may be contributed by the ferritic inserts and the test blanket modules [17]. The identification of reliable EF detection methods and the determination of robust EF control strategies in present magnetic fusion devices are of vital importance to guarantee the success of ITER and of next generation tokamaks.

In recent decades, in various experiments, such as Alcator C-mod [18], ASDEX Upgrade [19], COMPASS [20], DIII-D [21], EAST [22], EXTRAP-T2R [23], HBTP [24], KSTAR [25], JET [26], MAST [27], NSTX [28] and NSTX Upgrade [29], RFX-mod [30] and TCV [31], ad hoc studies have been performed to identify EF sources and to develop EF control strategies. These strategies, which aim to minimize the EF amplitude to the lowest value according to certain metrics, can involve passive and active EF control.

By passive EF control we mean the techniques that can be pursued when constructing or modifying the fusion device in order to compensate static EFs. For example, in the NSTX experiment a source of n=1 EF (n is the toroidal mode number) has been detected by the presence of a locked mode during plasma operations, resulting from a displacement of the central toroidal field coil bundle [28]. In particular, the displacement was caused by an electro-magnetic (EM) interaction between the toroidal

field and Ohmic heating coil. Passive EF control has been used to compensate this n=1 EF by placing mechanical shims between the toroidal field coil and the tension tube on which the Ohmic heating coil is wound in an attempt to reduce the motion of the toroidal field coil.

However, EFs minimization by passive control alone is not adequate for the compensation of EFs that have a time-varying behaviour, besides having a harmonic content which cannot be minimized by passive control. Therefore, fusion devices employ active coils, non-axisymmetric coils located in and/or ex-vessel, to reduce the magnetic field perturbations due to the EFs. Control algorithms, implemented in the plasma control system (PCS), can counteract such perturbations in real-time by feeding properly the active coils. This is how active EF control, or dynamic EF correction, works.

In the NSTX device, for example, active EF control has been used to minimize the residual n=1 EF after placing the mechanical shims and to reduce the n=3 EF associated with poloidal field coil manufacturing [28]. In DIII-D, active EF control is run in the PCS to compensate the intrinsic EFs due to the poloidal field coil misalignments and the busbars feeding the toroidal field coils [21, 32, 33]. In the RFX-mod device, active control has been employed to suppress EFs associated with the presence of a poloidal gap in the wall structure [30, 34]. In MAST, it has been used to reduce the intrinsic n=1 EF associated with the deformation of poloidal field coils [35, 36].

In this work, passive and active control strategies that have been adopted to compensate the EFs towards MAST Upgrade operation are presented.

MAST Upgrade [37, 38] has been built after a series of enhancements from the previous MAST device and it will be exploited in the near future. The main enhancement of MAST Upgrade consists of 4 new poloidal field coils (P), i.e. 2 coil pairs connected in series, and 14 divertor coils (D), i.e. 7 coil pairs connected in series, and a new closed pumped divertor structure which will allow investigation of various divertor configurations, i.e. Super-X, snowflake and long-inner leg. Figure 1 represents a sketch of MAST Upgrade poloidal section, where D and P coil sets are highlighted in blue and in red, respectively.

To guarantee a high quality experimental programme in terms of available operating space, operational robustness and good plasma performance, the presence of EFs in P and D coils has been investigated through high accuracy magnetic field measurements and corresponding 3D EM modelling. Such a study revealed that the main EFs have n=1 and n=2 harmonics.

Passive and active control strategies have been adopted to compensate these EFs. Passive EF control consisted in finding the optimal fine-scale coil alignment in order to minimize the n=1 EF. This is the only EF harmonic that can be compensated by shifting and tilting a coil. Conversely, active EF control will be employed for compensating the n=2 EF which is associated with P4 and P5 coil deformations. Since such coils have been re-used

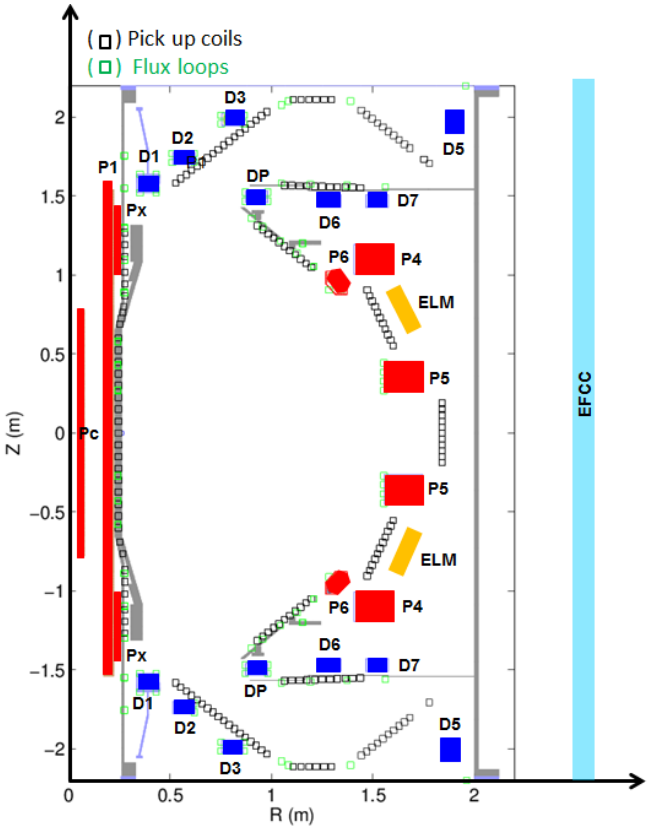

Figure 1: Sketch of the poloidal section of MAST Upgrade device where the P coils are highlighted in red, the D coils in blue, the ELM coils in orange and the EFCCs in light blue. In the same figure, the pick up coils and the flux loops are also reported with black and green squares, respectively.

from the MAST device, dedicated experiments on n=2 EF control have been performed during MAST operation to identify the best n=2 EF control technique. ERGOS [39] and MARS-F [40] codes have been used to interpret the experimental results and to perform a model-based optimization of the control parameters in preparation for EF control experiments in MAST Upgrade.

It is worth stressing that this study is not meant to be an exhaustive overview of all the EF sources present in MAST Upgrade, but it is based on the analysis of magnetic field measurements available when writing this document. We cannot exclude a priori the presence of other EF sources.

To detect spurious magnetic field perturbations, at the beginning of MAST Upgrade operation, the compass scan method [41, 42] will be employed. Such method relies on an active control system and a wide coverage of magnetic field sensors.

MAST Upgrade active control system consists of two sets of coils: the error field correction coils (EFCCs) and the edge localized mode (ELM) control coils [27]. The EFCCs and ELM control coil sets, which were previously installed in MAST device, are represented in figure 1 in light blue and in orange, respectively.

The EFCCs set consists of four coils arranged symmetrically around the outside of the MAST Upgrade vacuum vessel, located at R=2.9 m and Z=±2 m. Each coil is made up of 3 turns and can carry up to 5 kA/turn. The ELM coils set instead consists of 4 and 8 coils located above and below the outboard midplane of the torus, respectively. The actual number of ELM coils has been reduced with respect to MAST (6 and 12, respectively) due to the installation of an off-axis NBI system. Each ELM coil spans 0.270 m poloidally by 0.6 m toroidally and is composed of 4 turns. Thanks to the upgrade of the ELM coil power supplies, the current powers supply limit has been increased from 1.4, the MAST limit, to 2.1 kA.

An extensive coverage of magnetic field sensors, i.e. 354 pick up coils, 102 flux loops, 34 Mirnov coils, has been installed in MAST Upgrade to detect and control magnetic field perturbations associated with EFs and MHD modes, to control the plasma shape and position and to reconstruct the plasma equilibrium. The position of pick-up coils and flux loops is reported, as an example, in figure 1 with black and green squares, respectively.

The manuscript is structured as follows. Section II presents the methodology adopted to determine the optimal fine-scale coil alignment for the n=1 EF compensation. Section III deals with the best n=2 EF active control technique identified by analysing MAST experiments, where n=2 magnetic field perturbations have been applied by means of EFCCs and ELM coils, and by ERGOS studies. Section IV describes MARS-F modelling which has allowed the identification of optimization criteria for the best n=2 EF control strategy and to perform model-based tuning of the n=2 control parameters in preparation for MAST Upgrade EF studies. Section V gives the summary and the conclusions of the work.

II. PASSIVE n=1 EF CONTROL

Within MAST Upgrade project, the strategy that has been adopted to compensate the EFs associated with P and D coil deformations is to use the passive EF control during the assembly phase of the machine, rather than correcting them through active control during plasma operations.

To this aim, a characterization of EFs associated with P and D coils have been carried out by comparing high accuracy magnetic field measurements with 3D EM modelling, and a coil alignment optimization study has been investigated for their compensation.

Considering the P or the D coil as a rigid body, there are 6 degrees of freedom when positioning a coil within a device, namely displacement and rotation in and around each of three orthogonal directions (x, y, z), respectively. The convention for the x, y, z axis direction is indicated in figure 2.

However, not all of these movements were feasible when mounting a P or a D coil inside MAST Upgrade.

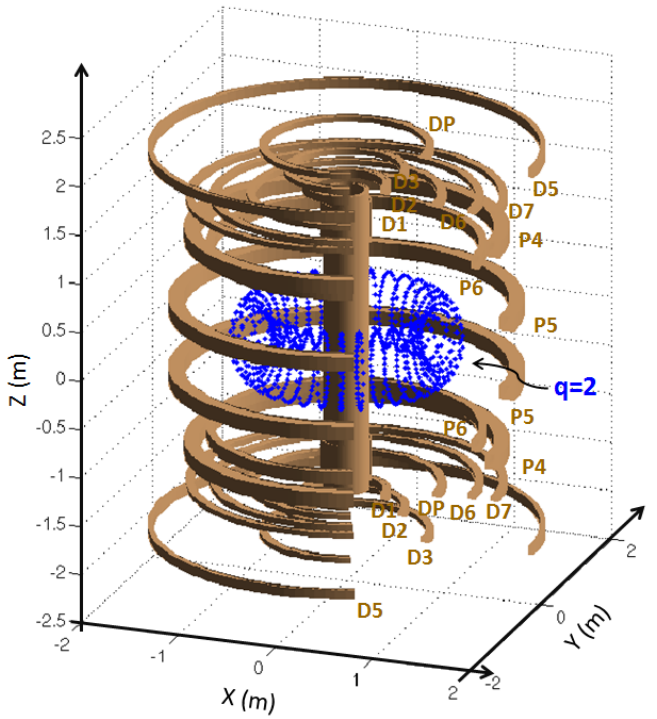

Figure 2: 3D model of MAST Upgrade P and D coil set and the location of the q=2 surface, in blue, in the A1 MAST Upgrade scenario, described in the text.

Due to engineering constraints, shifting the coil in both the x and y directions, of the order of some mm, and rotating it about both the x and y axes, of the order of some mrad, were the ones allowed. Only the n=1 EF harmonic can thus be compensated by passive control.

To understand how shifting or tilting a coil affects the n=1 magnetic field amplitude, a simplified 3D model of P and D coils has been used. Such 3D model, whose sketch is shown in figure 2, describes each coil as a single filament, assuming toroidal symmetry. The model being purely EM considers the vacuum approximation.

The effect of applying some coil movements on the n=1 magnetic field amplitude has been studied solving the Biot-Savart problem analysing the net field from two coils, one properly aligned and one misaligned, i.e. shifted or tilted, carrying opposite current. Notably, the n=1 magnetic field normal to the q=2, dubbed B_n, has been calculated. Among the magnetic surfaces, the q=2 has been chosen since it is the location of the 2/1 mode (m/n where m is the poloidal mode number), a deleterious plasma instability in fusion devices [7, 8].

The q=2 in the A1 MAST Upgrade scenario has been investigated. A1 is the main operational scenario that will be explored in the early phase of MAST Upgrade operation. A1 scenario is characterized by plasma current I_p=1.MA, equilibrium toroidal field B_0=0.78 T, the neutral beam power P_{NBI}=5 MW, the ratio between the plasma pressure and magnetic pressure $\beta = 2.5$, the safety factor on the axis $q_0 = 1.6$, the safety factor at 95%

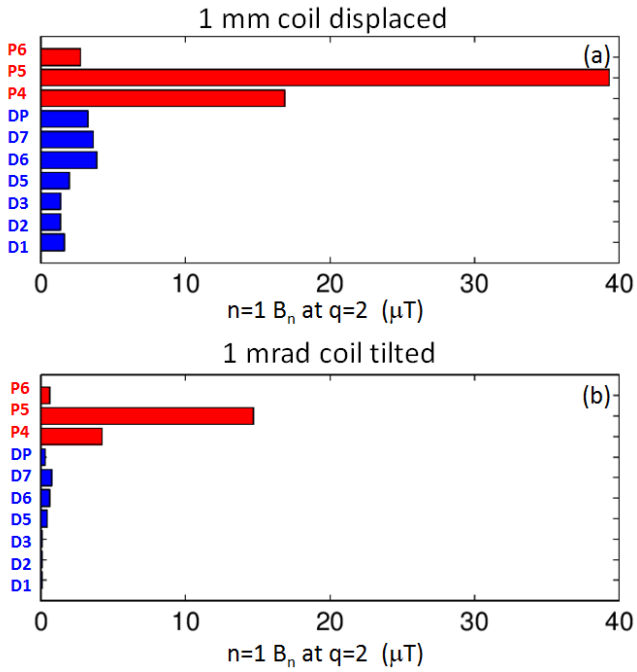

Figure 3: n=1 magnetic field amplitude in vacuum normal to the q=2 surface associated with P and D coils (a) 1 mm shifted and (b) 1 mrad tilted. The magnetic field amplitudes have been calculated considering the P and D coil currents foreseen in the A1 MAST Upgrade scenario.

Coil name	Current (kA)
D1	10
D2	10
D3	10
D5	7.5
D6	7.5
D7	7.5
DP	7.5
P4	18
P5	18
P6	8

Table I: D and P coil currents in A1 MAST Upgrade scenario.

of the radius $q_{95} = 10.1$. Such quantities have been calculated by predictive TRANSP calculations [43] while the corresponding magnetic field equilibrium by the EFIT code [44]. The position of the q=2 magnetic surface in A1 scenario is shown in blue in figure 2.

Figures 3(a)-(b) represent the calculated n=1 B_n amplitudes at q=2 associated with D coils and P coils 1 mm shifted and 1 mrad tilted, respectively.

This analysis shows that by shifting and by tilting a coil, an n=1 magnetic field can be created. Since the design and manufacturing processes of P and D coils can introduce an n=1 deformation, and thus an n=1 EF that

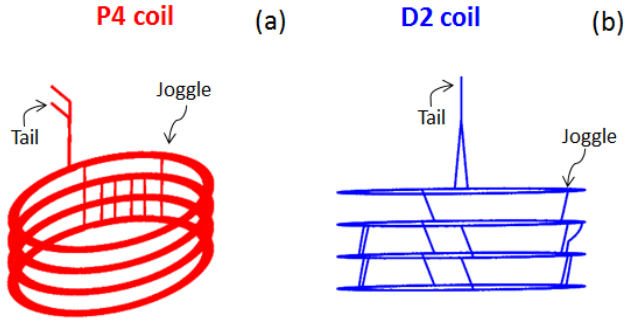

Figure 4: Design of (a) P4 coil and (b) D2 coil.

can affect plasma stability, the flexibility of adjusting the coil position can be exploited to induce an n=1 magnetic field for the n=1 EF compensation.

In particular, the results reported in figures 3(a)-(b) show that, independently of the coil movements, n=1 B_n amplitudes at q=2 associated with P4 and P5 coils are larger than the ones of D coils. Indeed, P4 and P5 coils are located closer to the q=2 surface and are fed by larger current levels than the D coil ones, as shown in table I where D and in P coil currents in A1 scenario are reported. This implies that an intrinsic n=1 EF in P4 and P5 coils could be more deleterious with respect to that one in D coils. Moreover, tilting the coils seems to be less effective for the n=1 EF compensation. The n=1 B_n amplitudes at q=2 associated with P and D coils 1 mm shifted are in fact larger than that ones associated with 1 mrad tilted.

This is important to point out that these conclusions have been drawn considering the vacuum approximation. The n=1 B_n at q=2 can significant change in the presence of plasma. For example, it can be amplified when exploring low plasma density regimes and high-β scenarios. In addition, the analysis has also been carried out considering a simplified description of the coil, i.e. a single filament, thus not including 3D coil deformations which would be present and responsible for EFs.

To identify the optimal coil alignment for the n=1 EF minimization, a realistic 3D coil geometry has to be employed. To this aim, 3D deformations of P and D coils associated with the coil design and from inaccuracies in the coil manufacturing process have been investigated.

P and D coils are not circularly symmetric even in the design since each turn has to make a transition from one layer to the next one. These connections are called joggles. The result is that in a coil which is notionally 6 turns by 4 turns, as the D2 coil and the P4 coil shown in figure 1, its design has only 23 turns, being the missing turn distributed through the coil. The design of P4 and D2 coils with the corresponding joggles is shown in figure 4(a)-(b), respectively.

Since joggles introduce a source of non-axisymmetry, EFs are intrinsically present in the design of the coil.

When facing the problem of finding the optimal coil

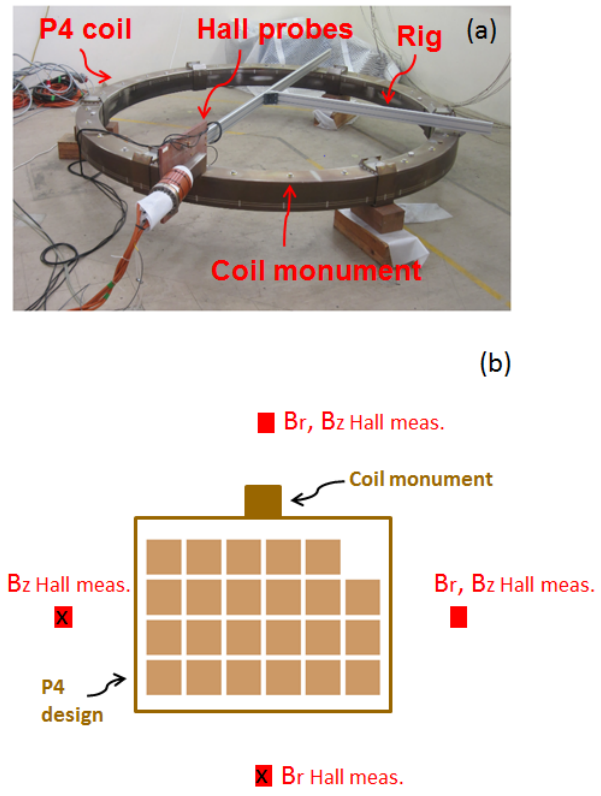

Figure 5: (a) Picture representing the moveable rig, the Hall probes placed on it and the P4 coil. (b) Sketch representing the P4 coil design, the position of the coil monument and the position of the Hall probes.

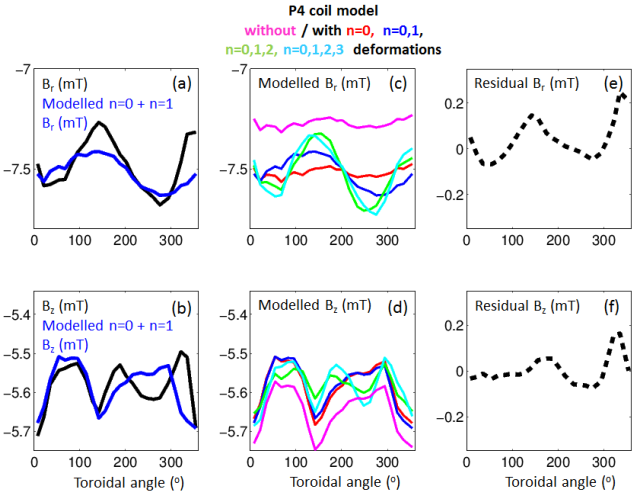

Figure 6: Toroidal distribution of the measured (a) radial and (b) vertical magnetic field components (in black) and the corresponding n=0 + n=1 magnetic field components from modelling (in blue). Toroidal distribution of the modelled (c) radial and (d) vertical magnetic field components calculated by the use of a single filament model of P4 coil without deformations (in magenta) and with $n = 0$ (in red), $n = 0, 1$ (in blue), $n = 0, 1, 2$ (in green), $n = 0, 1, 2, 3$ (in cyan) deformations. Toroidal distribution of the residual radial (e) and (f) vertical magnetic field components after n=0 and n=1 compensation.

alignment which reduces the intrinsic n=1 EF associated with the coil deformation, a question raises: shall we optimize the coil position to return it, as best possible, to its design state so without joggles or shall to try to minimize the designed-in EF? The second approach has been chosen since it seems worthwhile to minimize the EF as seen by the plasma rather than returning the coil to its as designed state.

The fine-scale alignment of P and D coils for the n=1 EF minimization has been assessed through high accuracy magnetic measurements and the associated 3D EM modelling. The methodology adopted to determine such coil alignment is reported, as an example, for a P coil, named P4.

To perform magnetic field measurements, 24 coil monuments were welded to the upper surface of the P4 coil case at approximately equal spacings and radius, and a moveable rig fixed the measurement positions of the magnetic field components precisely relative to these coil monuments.

The radial and vertical magnetic field components, i.e. B_r and B_z, of P4 coil have been measured by 3 high accuracy Hall probes mounted in the moveable rig, at 24 coil monument positions, therefore spanning every 15^o. In this way, more than 100 magnetic field measurements were available to characterize the 3D coil geometry.

A picture representing the moveable rig, the Hall probes and P4 coil is reported in figure 5(a).

The B_r and B_z measurements along the toroidal angle associated with P4 coil, fed by 250 A current, are shown in figures 6(a)-(b), respectively. This set of magnetic field measurements has been acquired by the Hall probes highlighted with a cross in the sketch of figure 5(b), which are about 0.2 m from P4 coil case.

Note that the B_r and B_z toroidal distributions have a complex structure which requires more than a single harmonic component to describe them. Therefore, intrinsic EFs associated with the coil design and manufacturing processes are present in P4 coil.

Because P4 coil case has 3D deformations, the magnetic field measurement positions were not uniformly spaced. Consequently, the magnetic field measurements are not per se useful. It is necessary to represent the coil by some model and then distort the coil model in some fashion to achieve a match to the magnetic field measurements at the actual measurement positions. The reference frame is then arbitrary, but was chosen to be a best-fit plane through the coil monuments positions centred at their centroid.

Initially a simple single filament coil model has been adopted for this study. The centre of the coil, whose radius is 1.5045 m, is placed at the coil monument centroid, which defines the (x, y) = (0, 0), and its vertical position is at z = 0.

The magnetic field map has been calculated by solving the Biot-Savart problem on the grid of points which corresponds to the Hall probe positions and and the modelled magnetic field has been compared with the corresponding experimental one.

The toroidal distributions of B_r and B_z calculated at the same positions of the magnetic field measurements reported in figures 6(a)-(b) are highlighted in magenta in figures 6(c)-(d), respectively.

Note that such magnetic field distributions are not flat. Being calculated at the coil monument positions, such distributions follow the shape of the coil case. Moreover, the modelled B_r and B_z along the toroidal angle are not around the mean values of the corresponding measured magnetic field components, as expected. There is at least 0.2 mT and 0.1 mT discrepancy, respectively. Such evidence suggests that the coil is not actually centred at the coil monument centroid.

In order to improve the agreement between the modelled and the measured magnetic field components, the single filament model of P4 coil has been deformed. From an analytical point of view, whatever coil deformations can be decomposed as a sum of different toroidal mode harmonics, n. The radial and vertical coordinates of the coil have been expressed as follows:

$$r = r_0 + \sum_{n=1}^{12} \delta_n^r cos(n\phi) + \sum_{n=1}^{12} \gamma_n^r sin(n\phi),$$

$$z = z_0 + \sum_{n=1}^{12} \delta_n^z cos(n\phi) + \sum_{n=1}^{12} \gamma_n^z sin(n\phi),$$

where r_0 and z_0 represent the radial and the vertical offsets that should be applied to identify the exact coil position, respectively. Instead, $\delta_n^r, \gamma_n^r, \delta_n^z, \gamma_n^z$ coefficients represent the radial and vertical deformations for each toroidal mode harmonic.

In the simplest case, $\delta_1^r, \gamma_1^r, \delta_1^z, \gamma_1^z$ represent a shift or tilt of the coil and thus produce a toroidal n = 1 asymmetry. Instead, $\delta_2^r, \gamma_2^r, \delta_2^z, \gamma_2^z$ correspond to a distortion from a flat circle, either in terms of an elliptic or out of plane bowing, and thus produce an n = 2 asymmetry. By increasing n, more complex deformations can be added to the single filament coil model. In particular, the n content of the applied deformations has been truncated to 12 since it is the maximum toroidal mode number that can be resolved with 24 magnetic field measurements available along the toroidal angle, without being affected by the aliasing problem.

A non-linear least squares algorithm has been used to find the r_0, z_0, $\delta_n^r, \gamma_n^r, \delta_n^z, \gamma_n^z$ parameters which bring the predicted B_r and B_z into agreement with the magnetic field measurements.

Figure 7 shows $\delta_n^r, \gamma_n^r, \delta_n^z, \gamma_n^z$ coefficients corresponding to n=1 (in blue), n=2 (in green) and n=3 (in cyan) radial and vertical deformations in P4 coil model. The

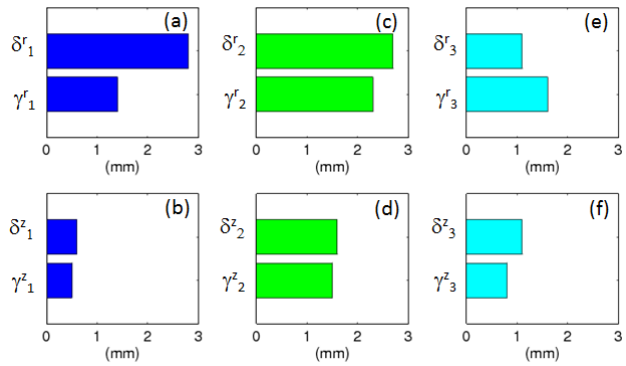

Figure 7: $\delta_n^r, \gamma_n^r, \delta_n^z, and \gamma_n^z$ coefficients considering n=1 (a-b), n=2 (c-d) and n=3 (e-f) radial and vertical deformations of P4 coil, respectively.

coefficients are shown for n up to 3, having the $n > 3$ coefficients smaller amplitudes. Such coefficients have been used to calculate the radial and vertical magnetic field components considering different n deformations in the single filament coil model.

The toroidal distributions of B_r and B_z calculated at the same position of the corresponding magnetic field measurements are reported in figures 6(c)-(d), considering the coil model n=0 compensated, i.e. the coil model has been corrected by radial and vertical offsets (in red), and considering the coil model distorted with n up to 1 (in blue), with n up to 2 (in green) and with n up to 3 (in cyan).

To achieve a good agreement between the measured magnetic field components and the modelled ones, the single filament coil model should accommodate deformations with at least n up to 2. In other words the P4 coil geometry is characterized by the presence of mainly n=1 and n=2 EFs. A similar conclusion has been drawn previously when magnetic field measurements of P4 (and P5 as well) have been performed by the use of a clamp ring devised inside MAST [27, 35].

The n=1 EF harmonic can be minimized by identifying the optimal fine-scale alignment of P4 coil inside MAST Upgrade device. To this aim, the $\delta_{n=1}^r, \gamma_{n=1}^r, \delta_{n=1}^z, \gamma_{n=1}^z$ coefficients have been used, in combination with the toroidal location of P4 tail, to calculate the P4 coil monument coordinates for the assembly within MAST Upgrade device. Note that the optimal coil alignment has been determined by using a simplified coil model, which takes into account only the n=1 coil deformation accordingly to the magnetic field measurements, thus neglecting presence of coil tail and joggles.

To assess the importance of including such 3D coil features, the actual P4 design model, shown in figure 4(a), has been used for the Biot-Savart calculation, instead of the n=1 distorted single filament coil model, and the coil monument coordinates have been calculated for the coil assembly.

Such coordinates are very similar to the ones identi-

fied by the use of the n=1 deformed single filament coil model. Despite the use of different coil models, the good agreement in determining the optimal coil alignment for the n=1 EF compensation is due to the fact that the joggles and the coil tail are features very localized toroidally in P4 coil design, as shown in figure 4(b). In this case, high-n harmonic deformations should be used to describe them. The coil position alignment, being focused on the n=1 EF harmonic only, is not altered by high-n harmonics.

Clamps have been adopted to finely position and rotate P4 coil inside the device and, once the coil has been installed in the lower midplane of MAST Upgrade, as shown in figure 1, the coordinates of the coil monuments have been rigorously checked by photogrammetry.

By the proper alignment of P4 coil, the toroidal distributions of B_r and B_z, shown in blue in figure 7(a)-(b), respectively, can be minimized. By subtracting these quantities from the corresponding measurements, the residual B_r and B_z have been calculated and reported in figures 6(e)-(f), respectively.

Note that such magnetic field distributions highlight the presence of an n=2 deformation in the P4 coil, expecially along the radial coordinate. Since the n=2 EF cannot be compensated by passive control in MAST Upgrade, active EF control will be employed for the n=2 EF minimization, as described in the following section.

A coil alignment optimization study, similar to the one presented here for P4 coil, has been carried out for the other P coils shown in figure 1 excluding P1, Pc and Px which cannot be moved because of engineering constraints. On the other hand, the investigation of D coil deformations through magnetic field measurements will be reported in a separate paper [38] together with the optimal D coil alignment for the n=1 EF compensation.

The n=1 EF passive control strategy adopted to compensate the n=1 EF associated with P and D coil deformations should minimize the occurrence of plasma terminations caused by n=1 EF driven locked mode during MAST Upgrade experiments.

However, plasma terminations could still occur, especially when exploring regimes where the plasma is more prone to EFs, because of the presence of partially uncompensated n=1 EFs by passive control and/or other unknown n=1 EF sources. Such EFs could also have a time-dependent behaviour. If the n=1 EF amplitude, measured by the compass scan, is not negligible, being MAST Upgrade equipped with in and ex-vessel active coils, active control schemes will be employed for its minimization.

III. ACTIVE n=2 EF CONTROL

During MAST operation, the intrinsic n=1 EF associated with P4 and P5 coil deformations has been compensated by active control. n=1 EF control has allowed to explore density 30% lower than that one achievable otherwise and this density was still not low enough for a locked mode to occur [35, 36].

In MAST Upgrade, the n=1 EF amplitude has been reduced by tailoring P4 and P5 coil positions when building the new device, as described in the previous section. However, an uncompensated n=2 EF is still present, associated with these coil deformations, as documented in [27, 35], and as discussed previously, for the case of P4 coil. Conversely, no n=2 EFs have been detected by analyzing magnetic field measurements of D coils.

Since similar levels of plasma rotation braking and performance degradation have been observed in the presence of n=1 and n=2 magnetic field errors [46–52], in preparation for MAST Upgrade exploitation, the development of a proper control strategy for the n=2 EF associated with P4 and P5 deformations is important.

The experience gained during MAST operation on n=2 EF control has been used to understand the effect of such EF on the plasma dynamic and to have highlights on its active control.

Evidence of an n=2 EF

First experiments on ELM control used the EFCCs system to induce 3D n=2 magnetic fields. Although this topic is beyond the scope of the present work, these experiments are interesting per se since they have highlighted the presence on an n=2 EF and allowed to study its effect on the plasma performance.

Figures 8(a-b-c) represent similar I_p = 0.7 MA single null divertor (SND) plasmas, as shown by the time behaviour of the plasma density, the toroidal rotation in the core and at the edge, as measured by charge exchange recombination spectroscopy diagnostic (CXRS) and D_α emission. In all the experiments, 3.3 MW NBI power (not shown here) has been injected starting from t=0.1 s. Notably, the experiment highlighted in black is the reference plasma. Here, the intrinsic n=1 EF has been controlled by feedforward currents in the ELM coils [35, 36], as shown in figure 8(e). The other discharges have in addition n=2 magnetic field perturbations applied by means of EFCCs.

The EFCCs system, being equipped with 4 coils and 2 powers supplies, enables us to set two n=2 magnetic field configurations. The associated 3D n=2 magnetic fields, which differ by 90^o phase shift, can have a toroidal pattern as the blue trace in figure 9(a), which corresponds to an n=2 magnetic field perturbation with $\phi_{EFCC} = 0^o$, or as the blue trace, which corresponds to an n=2 magnetic field perturbation with $\phi_{EFCC} = 90^o$.

In particular, these traces represent the toroidal distribution of the n=2 radial magnetic field, at R=1.45 m and Z=0 m, calculated by the ERGOS code [39]. ERGOS is an EM modelling tool which solves the Biot-Savart law given a realistic description of the EFCCs, ELM coils and P4 and P5 coils geometry and the current polarity connections among the active coils. It calculates the

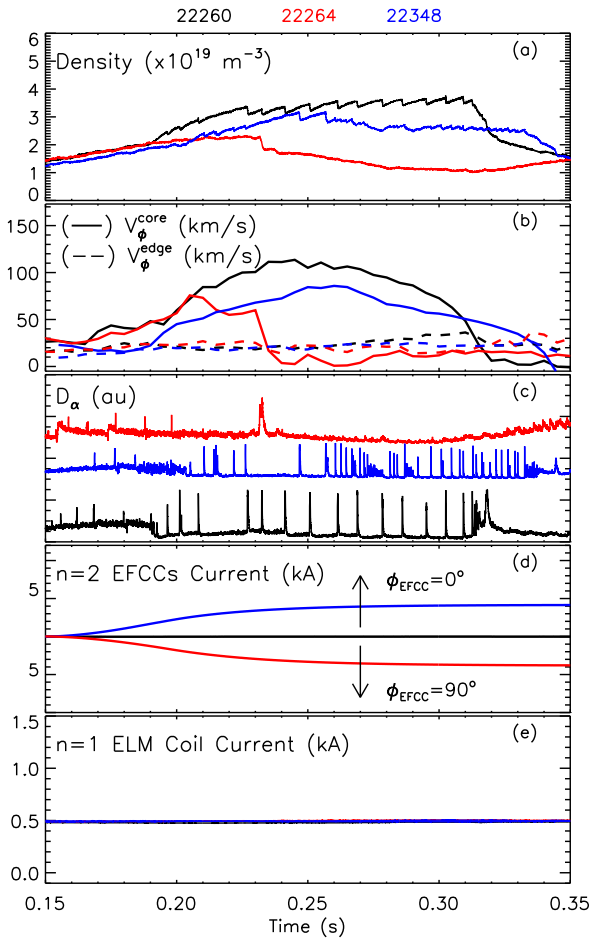

Figure 8: Time behaviour of (a) electron density, (b) toroidal rotation in the core, at R=1.2 m (solid line) and at the edge, at R=1.37 m (dashed line) (c) D_α, (d) n=2 EFCCs current and (e) n=1 ELM coil current of a plasma experiment with n=1 EF control only by means of ELM coils (in black), with n=1 EF control by means of ELM coils plus an n=2 magnetic field perturbation induced by EFCCs with 0^o (in red) and 90^o(in blue) toroidal phases.

associated 3D magnetic fields, it adds them together according to the current level in each coil and finally it combines them with the plasma equilibrium field. For this study, the plasma equilibrium of 21585 discharge, an experiment similar to the reference plasma, at t=0.24 s has been calculated by the EFIT equilibrium code [44].

The time behaviour of n=2 EFCCs current is reported in figure 8(d). The plasmas plotted in blue and in red have an externally applied n=2 magnetic field perturbation with the same amplitude but different toroidal phase, i.e. $\phi_{EFCC} = 0^o$ and $\phi_{EFCC} = 90^o$, respectively. Table II summarizes the EFCCs parameters used in these experiments.

3D n=2 magnetic fields applied by means of EFCCs do not affect the radial profiles of density and temperature (not shown), which are very similar to the reference plasma during the penetration phase of the external magnetic field. Conversely, such n=2 magnetic field perturbations significantly influence the core toroidal rotation.

Shot	I_{EFCC} (kA)	ϕ_{EFCC} (^{o})	Rotation rating
22260	0	0	+ +
22264	3.9	0	- -
22348	3.9	90	-

Table II: EFCCs control parameters tested in the plasmas in figure 8 and the corresponding ratings on plasma rotation sustainment/braking. The plasma rotation is well sustained (+ +) in the reference plasma, i.e. without the n=2 magnetic field, conversely the plasmas with external n=2 3D magnetic field has modest (-) or large rotation braking (- -) depending on the EFCCs control parameters applied.

At t=0.15 s, before the application of the external n=2 magnetic field, the plasma rotation, both in the core (solid line) and at the edge (dashed line), is very similar among the plasmas analysed, as shown in figure 8(b). As soon as the n=2 magnetic field perturbation with $\phi_{EFCC} = 0^o$ is applied, the toroidal rotation in the core brakes and a reduction of about $30-40\%$ is observed with respect to the reference plasma. The rotation braking is localized in the core, not at the edge, similar to what has been observed in other tokamak experiments [46, 53, 54]. Conversely, when the n=2 magnetic field perturbation with $\phi_{EFCC} = 90^o$ is applied, until t=0.21 s, no effect on the core rotation has been observed. Afterward, the core rotation is drastically reduced because of the triggering of a locked mode. Similar to the previous case, the edge rotation is not affected by the presence of the external n=2 magnetic field.

Although it is not the aim of this work studying the effect of n=2 magnetic field perturbations on ELMs dynamic, it is worth mentioning that the ELMs are more frequent and irregular in the plasma which has an n=2 magnetic field perturbation with $\phi_{EFCC} = 90^o$ with respect to the reference plasma, as shown by the time behaviour of D_α reported in figure 8(c). Conversely, no ELMs have been observed in the experiment which has an n=2 magnetic field perturbation with $\phi_{EFCC} = 0^o$ since it never enters in H-mode due to the presence of the locked mode.

The clear difference in the length of the high plasma performance phase between the discharges with externally applied n=2 magnetic field perturbations highlights the presence of an intrinsic n=2 EF in MAST, as expected by P4 and P5 coil deformations.

The ERGOS code has been used to interpret these experimental evidences. Figure 9(a) shows in black the calculated toroidal distribution of the radial magnetic field, at R=1.45 m and Z=0 m, of the intrinsic EF n=1 compensated by means of ELM coils. This quantity corresponds to the radial magnetic field distribution of the reference plasma. Note that a clear n=2 patter can be detected in such radial magnetic field distribution, which is due to the presence of an uncompensated n=2 compo-

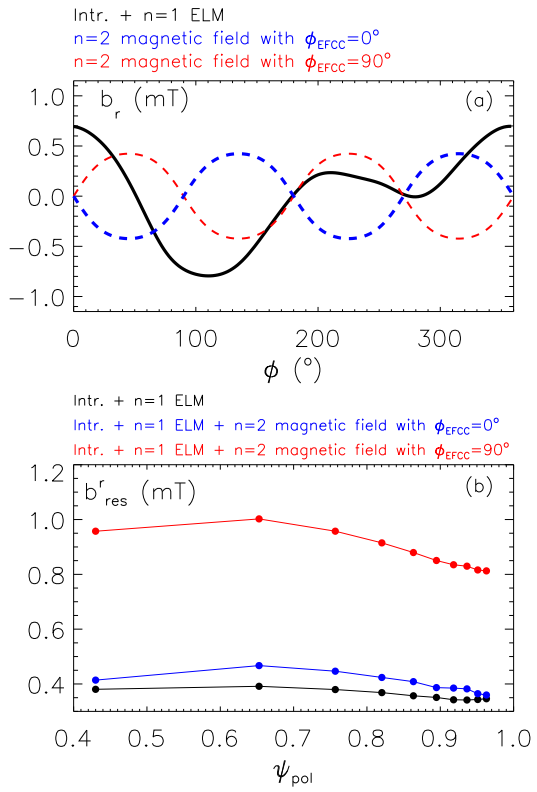

Figure 9: (a) Toroidal distribution of the mean radial magnetic field perturbation at R=1.45 m and Z=0 m associated with the n=1 compensated intrinsic EF by means of ELM coils (in black), the 3D n=2 magnetic field by means of EFCCs with $\phi_{EFCC} = 0^o$ (red) and $\phi_{EFCC} = 90^o$ (blue). (b) Radial profiles of the n=2 resonant magnetic field components associated with the n=1 compensated intrinsic EF (in black), the n=1 compensated intrinsic EF plus an n=2 magnetic field perturbation with $\phi_{EFCC} = 0^o$ (in blue) and the n=1 compensated intrinsic EF plus an n=2 magnetic field perturbation with $\phi_{EFCC} = 90^o$ (in red).

nent in the intrinsic EF.

The n=2 EF amplitude can be amplified or minimized by an external 3D n=2 magnetic field depending on the relative phase alignment between such external perturbation and the n=1 compensated intrinsic EF.

The ERGOS code predicts that the external n=2 magnetic field perturbation with $\phi_{EFCC} = 90^o$ has the worst phase alignment for the n=2 EF control. This is clear by comparing the black and the red traces in figure 9(a). Being the n=2 radial magnetic fields with $\phi_{EFCC} = 90^o$ aligned for some toroidal positions with the n=1 compensated intrinsic EF, an amplification of the n=2 EF amplitude is foreseen when this external n=2 magnetic field is applied. Conversely, the external n=2 magnetic field perturbation with $\phi_{EFCC} = 0^o$ is slightly better misaligned with respect to the n=1 compensated intrinsic EF, as deduced by comparing the black and the blue traces in figure 9(a), and this misalignment could be beneficial for the n=2 EF compensation.

However, ERGOS modelling of the n=2 normalized resonant magnetic field components, b^r_{res}, defined as the ratio between the magnetic field perturbation in the direction perpendicular to the flux surfaces and the toroidal field [35], shows that external n=2 magnetic field perturbations induced by EFCCs are not effective in reducing the n=2 EF amplitude.

Figure 9(b) shows how the n=2 b^r_{res} varies as a function of the normalized equilibrium poloidal flux, ψ_p. The radial profile of b^r_{res} reported in black corresponds to the n=1 compensated intrinsic EF by means of ELM coils, the one in blue the n=1 compensated intrinsic EF plus an n=2 magnetic field perturbation with $\phi_{EFCC} = 0^o$, and the one in red the n=1 compensated intrinsic EF plus an n=2 magnetic field perturbation with $\phi_{EFCC} = 90^o$.

The ERGOS code suggests that when an n=2 magnetic field perturbation with $\phi_{EFCC} = 90^o$ is applied, the radial profile of b^r_{res} is more than twice larger than that one without the external n=2 magnetic field perturbation. In this case, the externally applied n=2 magnetic field, being phase aligned with the n=2 EF pattern, amplifies the n=2 EF amplitude. This is the reason why a locked mode and a strong rotation braking have been observed in the plasma plotted in red in figure 8.

On the other hand, when an n=2 magnetic field with $\phi_{EFCC} = 0^o$ is applied, the radial profile of b^r_{res} is significantly reduced with respect to the previous case. However, the radial profile of b^r_{res} is still larger than that one without the external n=2 magnetic field perturbation, as shown by comparing the black and the blue traces in figure 9(b). The braking of plasma rotation in the discharge plotted in blue in figure 8, which has an n=2 3D magnetic field with $\phi_{EFCC} = 90^o$, can thus be associated with the increase of the n=2 EF amplitude.

Based on these experimental and modelling results we can conclude that with the phase alignment between the n=1 compensated intrinsic EF and the 3D n=2 magnetic fields induced by the EFCCs system not being optimal, a proper n=2 EF minimization cannot be guaranteed by the use of EFCCs set. This limitation is due to the fact that the EFCCs system is equipped with 4 coils and only 2 power supplies. Upgrading the EFCCs system by feeding each coil independently could allow more flexibility in adjusting the phase between the external n=2 magnetic field perturbation and the n=1 compensated intrinsic EF, and thus could improve n=2 EF control.

n=2 EF correction by ELM coils

The experimental results and the corresponding modelling described in the previous subsection have demonstrated that it is important to take into account the spatial distribution of the intrinsic EF in experiments aiming at its compensation. This is achieved by optimizing the phase alignment between the magnetic field perturbation associated with the EF and the external 3D magnetic field.

It is worth mentioning that the fine tuning of the phase alignment is part of the control optimization effort not only in EF control studies, such as the ones discussed in this paper and in [35], but also in experiments aiming on ELM [36, 55–57] and tearing mode control [58].

In order to attempt the intrinsic n=2 EF control, the ELM coil system has been employed since, being equipped with a larger number of active coils and power supplies with respect to the EFCCs system, it offers more flexibility in tuning the phase alignment. Moreover, the ELM coils set has also the advantage to be located inside the vacuum vessel. Therefore, the associated magnetic field is not delayed and distorted by the penetration through the passive structure.

The ERGOS code has been extensively used to seek the best ELM coil control parameters which minimize the resonant magnetic field of the intrinsic EF at the q=2 surface. With the ERGOS code being based solely on an EM model, this EF optimization criterion is valid in vacuum condition.

The n=2 EF control strategy has been developed for various MAST plasma scenarios. The one reported here corresponds to a I_p = 0.6 MA SND plasma. The SND configuration has been chosen since it has been used previously in MAST EF experiments so the optimal n=1 EF control by means of EFCCS is well known [35, 36]. Being the SND plasma shifted downward, the lower ELM coils row only has been employed for n=2 EF control.

The toroidal distribution of the radial magnetic field pattern that should be n=2 compensated by the ELM coils is shown in figure 10(a) in black. This quantity has been calculated by the ERGOS code considering the magnetic fields associated with P4 and P5 coil and EFCCs geometry and the corresponding active coil connections [35] and corresponds to the intrinsic EF n=1 corrected by the EFCCs at R=1.45 m and Z=0 m. Note that this radial magnetic field distribution is quite similar to the black curve in figure 9(b), which represents the same quantity associated with the intrinsic EF n=1 compensated by the ELM coils, instead of the EFCCs.

Different ELM coil control parameters have been tested in the ERGOS code looking for the n=2 magnetic field perturbation which has the optimal amplitude and phase for the compensation of the intrinsic n=2 EF.

Notably, the ELM coil current, I_{ELM}, which determines the amplitude of the external 3D n=2 magnetic field, has been varied within a restricted range, considering the following values I_{ELM} (kA) = [0.5, 1, 1.2]. On the other hand, the ELM coil phase, ϕ_{ELM}, which represents the toroidal phase shift of the n=2 magnetic field perturbation with respect to the location of sector 1 in MAST [35] has been scanned within $0^o < \phi_{ELM} < 180^o$ because of the n=2 periodicity. Such ELM coil control parameter can be adjusted changing the current polarity distribution in the lower ELM coils row.

Figure 10(b) shows the toroidal distribution of the n=2 radial magnetic field, at R=1.45 m, Z=0 m, associated with n=2 magnetic field perturbations with 0.5 kA ELM

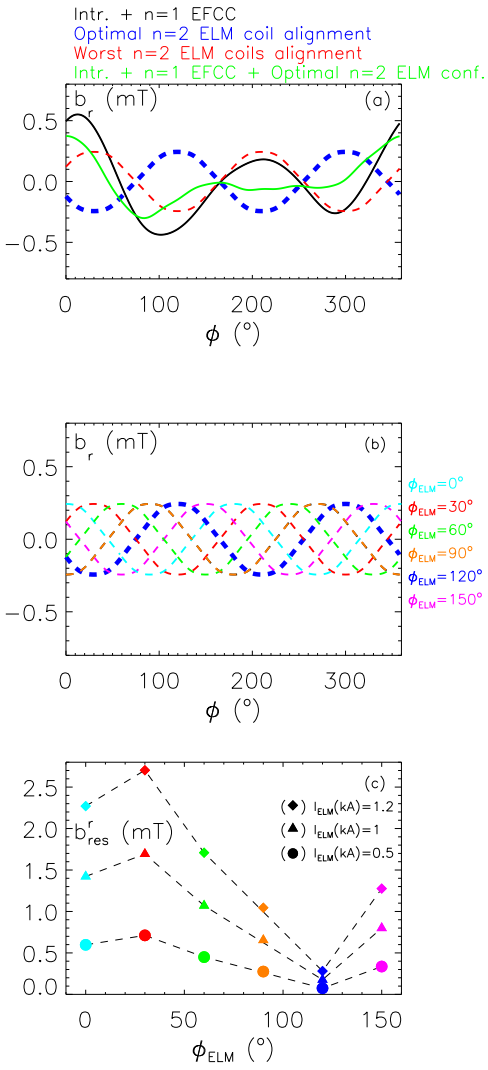

Figure 10: (a) Toroidal distribution of the radial magnetic field, at R=1.45 m, Z=0 m, associated with the n=1 compensated intrinsic EF by means of EFCCs (in black), the optimal (in blue) and the worst (in red) ELMs coil alignment for the n=2 EF control and the residual EF amplitude once compensated for both the n=1 and n=2 EFs (in green). (b) Toroidal distribution of the n=2 radial magnetic field induced by 0.5 kA ELM coil current and different ELM toroidal phases. (c) Resonant radial magnetic field amplitude at q=2 as a function of ϕ_{ELM} and at various I_{ELM}.

coil current but with different ϕ_{ELM}. The color code has been used to distinguish the various ELM coil phases. Note that the variation step in the ELM coil phase scan is 30^o because 12 coils were present in the lower ELM coils row.

Among the various ELM coil phases tested in the ERGOS code, the use of $\phi_{ELM} = 120^o$ allows the phase alignment between the n=1 compensated intrinsic EF and the external n=2 magnetic field perturbation be-

ing the optimal for the n=2 EF compensation. The black and the blue traces in figure 10(a), which represent the aforementioned quantities, respectively, are in fact out of phase, which is the most effective phase misalignment for n=2 EF compensation. Conversely, the use of $\phi_{ELM} = 30^o$ allows for the worst phase alignment for the n=2 EF control. In this case, the the n=1 compensated intrinsic EF is lined up with the external n=2 magnetic field perturbation, as shown by comparing the black and the red traces in figure 10(a). If an external n=2 perturbation with $\phi_{ELM} = 30^o$ had been applied in a plasma experiment, an amplification of the n=2 EF is expected.

Among the various ELM coil current amplitudes tested in ERGOS, I_{ELM}=0.5 kA is the optimal current value for n=2 EF control since it allows, in combination with the use of $\phi_{ELM} = 120^o$, the resonant radial magnetic field amplitude at q=2 for being the lowest. This is shown in figure 10(c) which represents how b^r_{res} at q=2 scales as a function of the toroidal phase of the external n=2 magnetic field, for different ELM coil current amplitudes. Various colors have been used to distinguish different ϕ_{ELM}. Instead, various symbols have been used to highlight different I_{ELM}.

By the use of the optimal n=2 EF control by means of ELM coils, i.e. I_{ELM}=0.5 kA and $\phi_{ELM} = 120^o$, in combination with n=1 EF control by means of EFCCs, ERGOS modelling foresees a reduction of the EF amplitude with respect to the case with n=1 EF compensation, only. This is shown in figure 10(a), where the toroidal distribution of the radial magnetic field, at R=1.45 m and Z=0 m, associated with the above mentioned quantities are reported in green and in black, respectively.

It is important to point out that the reduction of the EF amplitude by means of multi n-EFs control has been predicted considering the vacuum approximation. In the presence of plasma, n=1 and n=2 EF amplitudes could be amplified when exploring low density regimes [1] and high-β [15, 16], or it could be reduced because of the rotation shielding effect.

To test ERGOS predictions, the first attempt of controlling the n=2 EF by means of ELM coils has been performed during MAST operation, while correcting the n=1 EF through the EFCCs system. These experiments, besides providing ERGOS code validation, allowed to study the effect of an n=2 EF on plasma performance and to acquire expertise on its control, by testing different control strategies, in preparation for MAST Upgrade EF studies.

The figure of merit that has been used to define a successful n=2 EF control strategy is the sustainment of the plasma rotation. This quantity in fact represents the effectiveness of the EF control strategy in reducing the n=2 EF amplitude, avoiding mode locking.

n=2 EF control has been attempted in I_p = 0.6 MA SND plasma scenario, the same scenario investigated in the ERGOS simulations described previously. The experiments analysed have similar plasma parameters, as

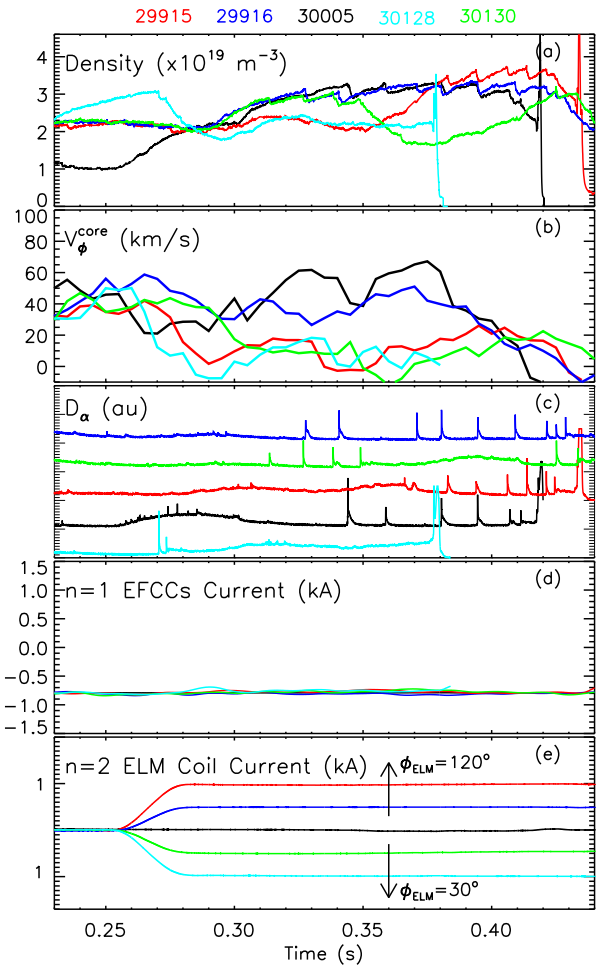

Figure 11: Time behaviour of (a) electron density, (b) core plasma rotation, at R=1.2 m, (c) D_α emission, (d) n=1 EFCCs current, (e) n=2 ELM coil current of a plasma experiment without (in black) and with (different colors) n=2 magnetic field perturbations. The color code has been used to distinguish n=2 magnetic field perturbations with different amplitudes and toroidal phases. The ELM coil control parameters used in these plasmas are summarized in table III.

shown by the time behaviour of plasma density and D_α emission, shown in figures 11 (a) and (c), respectively. In all the experiments, 4 MW NBI power (not shown here) has been injected starting from t=0.1 s and the intrinsic n=1 EF has been real-time compensated by means of EFCCs, as shown by the time behaviour of n=1 EFCCs current reported in figure 11(d).

Various ELM coil control parameters have been tested in these plasmas in order to identify the optimal n=2 EF control strategy. The time behaviour of n=2 ELM coil current is shown in figure 11(e). In particular, the plasma in black has no externally applied n=2 magnetic field perturbation and it represents the reference plasma. The other plasmas have externally applied n=2 magnetic field perturbations with ELM coil control parameters as

Shot	I_{ELM} (kA)	ϕ_{ELM} (^{o})	Rotation rating
30005	0	0	+ +
29916	0.5	120	+
29915	1	120	-
30130	0.5	30	-
30128	1	30	- -

Table III: ELM coil control parameters for n=2 EF compensation tested in the plasmas in figure 11 and the corresponding ratings on plasma rotation sustainment/braking. The plasma rotation is well sustained (+ +) in the reference plasma, i.e. without the n=2 magnetic field, conversely, among the plasmas with external n=2 ED magnetic field, the largest rotation braking (- -) has been obtained when the largest ELM coil current amplitude and the worst ELM coil alignment have been applied. Intermediate levels of rotation braking (-) and sustainment (+) have been obtained by the use of different combination of ELM coil current and ELM coil phase.

listed in table III.

Similarly to what has been observed in plasmas with n=2 magnetic field perturbations induced by means of EFCCs, n=2 magnetic field perturbations by means of ELM coils affect mainly the core rotation.

Around t=0.25 s, before the application of the n=2 magnetic field perturbation, the core rotation is similar among the plasmas, as shown in figure 11(b). The reference plasma has a core rotation of around 50 km/s before t=0.38 s. Afterwards, a locked mode is triggered and the rotation brakes. The presence of the locked mode could be associated with a partially uncompensated n=1 magnetic field error by EFCCs. Because of the 0.005 s time resolution of CXRS diagnostic, it is not straightforward to untangle if the rotation slowing down is associated with the locked mode, or viceversa if the locked mode is triggered because of the decrease of magnetic shielding effect by plasma rotation. Further investigations on this topic are ongoing and will be reported in a separate paper.

The plasmas with externally applied n=2 magnetic fields experience different levels of rotation braking as soon as the ELM coil current is ramped up. Notably, the plasma with the largest rotation braking is the one highlighted in cyan in figure 11(b). In this plasma, I_{ELM}=1 kA and $\phi_{ELM} = 30^o$ have been used as ELM coil control parameters. Conversely, the plasma with the lowest rotation braking is the one highlighted in blue. In this experiment, I_{ELM}=0.5 kA and $\phi_{ELM} = 120^o$ have been applied. On the other hand, the plasmas, plotted in green and in red, experience an intermediate rotation braking. A rating overview of the rotation sustainment/braking of the plasmas presented in figure 11 has been reported in the right column of table III.

This set of experiments conveys that the rotation braking is larger in plasmas with I_{ELM}=1 kA with respect to that ones with I_{ELM}=0.5 kA, as shown by comparing the red with the blue trace or the cyan with the green trace in figure 11(b). This experimental evidence is consistent with ERGOS modelling which predicts an increase of b_{res} at q=2 by increasing I_{ELM}, as reported in figure 10(c). Moreover, the plasmas which used $\phi_{ELM} = 30^o$ experience a rotation braking stronger than that one in plasmas which used $\phi_{ELM} = 120^o$, as shown by comparing the green with the blue trace or the cyan with the red trace in figure 11(b). Also this insight agrees with ERGOS modelling results reported in figure 10(c), which foresee a minimum b_{res} at q=2 when $\phi_{ELM} = 120^o$.

Among the ELM coil control parameters for n=2 EF control tested, I_{ELM}=0.5 kA and $\phi_{ELM} = 120^o$, used in the discharge plotted in blue in figure 11, are the best ones in reducing the n=2 EF since they allowed for the lowest rotation braking. This evidence is consistent with ERGOS predictions which foresee the minimization of b_{res} at q=2 when such ELM coil control set is used. I_{ELM}=0.5 kA and $\phi_{ELM} = 120^o$ have been thus dubbed the best ELM coil control set for the n=2 EF correction.

MARS-F modelling studies [40], carried out after performing these experiments and described in details in the next section, reveal that actually the best ELM coil control set is not the true optimal one. The I_{ELM} used experimentally is overestimated with respect to that ones foreseen by the MARS-F code, for the same n=2 EF optimization criterion. The true empirical optimal set would only be identified if a finer ELM coil current amplitude scan has been performed during the design phase of the n=2 EF control experiments, by the use of ERGOS code, or during the n=2 EF control experiments, as well. Such detail scan has not been carried out because of the limited experimental time available for this study during MAST operation.

The use of the not true optimal I_{ELM} in the plasma with the best ELM coil control set can explain why a rotation braking, of about $10 - 20\%$ with respect to the reference plasma, has been observed before t=0.38 s, time instant in which, analogously to the reference plasma, a n=1 locked mode is triggered.

To identify the optimization criteria the best n=2 EF control strategy fulfils considering also the plasma response, the MARS-F code has been used. This is the topic of the next section, together with the use of MARS-F code to fine-tune the n=2 EF control in preparation for MAST Upgrade EF control studies.

IV. THE USE OF MARS-F FOR FINE-TUNING THE n=2 EF CONTROL

The MARS-F code [40] is a linear single fluid MHD code, in full toroidal geometry, that combines the plasma response with the vacuum perturbations, including the screening effects due to toroidal rotation.

This code has been used in [36] to understand which control criteria the optimal n=1 EF control strategy, empirically identified, fulfils. Here, analogously, the MARS-F code has been used to interpret the experimental re-

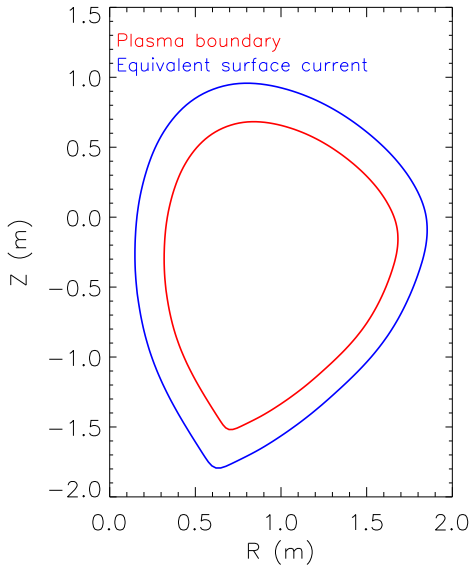

Figure 12: Plasma boundary (in red) and the surface where MARS-F calculates the equivalent current source (in blue). The quantities refer to 29916 discharge, at t=0.35 s. In this experiment the best ELM coil control set has been used.

sults on n=2 EF control by comparing the predicted optimal ELM coil control parameters, for multiple optimization criteria, with the best ELM coil control parameters, empirically identified.

For this study, similar to [36], the intrinsic n=2 EF associated with the P4 and P5 deformations has to be represented by an equivalent surface current in the MARS-F code. By defining this quantity we are able to study the response of the plasma to the intrinsic n=2 EF.

Since we are interested on the n=2 EF control, this harmonic alone is included in the study. The EF control problem is in fact treated linearly, so there is no coupling between the intrinsic n=1 and n=2 EFs which can be separately investigated without affecting the final computational results [36].

For this analysis, the plasma equilibrium of 29916 discharge, in which the best n=2 EF control strategy has been used, has been constructed at t=0.35 s by the EFIT code.

For the calculation of the equivalent surface current, the MARS-F code requires as input the normal magnetic field of the n=2 EF source. This quantity has been calculated by the ERGOS code. Figure 12 shows the plasma boundary and the surface where MARS-F calculates the equivalent current source, plotted in red and in blue, respectively.

To identify which optimization criteria the empirically identified n=2 EF correction fulfils, the combination of the intrinsic n=2 EF and the ELM magnetic fields has been considered, aiming at identifying the ELM coil control parameters which minimize the target quantity according to a certain criterion.

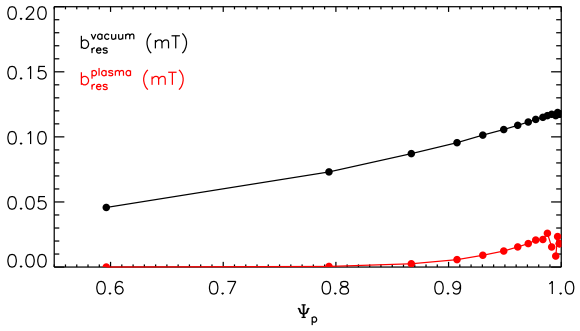

Figure 13: Resonant n=2 components of the vacuum field (in black) and the full field including the plasma response (in red) predicted by the MARS-F modelling.

For the plasma response calculations, MARS-F code uses as inputs the experimental radial profiles of plasma density and temperature from Thomson scattering diagnostic and the toroidal rotation from CXRS.

In the following, the n=2 EF optimization criteria that have been investigated through MARS-F modelling are briefly described.

- Full cancellation of the n=2 resonant magnetic field in vacuum and in the presence of plasma

  Similar to [35, 36], we have investigated the ELM coil control parameters which cancel the resonant n=2 magnetic field, obtained summing the EF and the ELM field. The resonant n=2 magnetic field should be nulled either at a certain magnetic field surface or its mean value, considering either the cancellation of the vacuum field only and that of the full field, which includes also the plasma response.

  In this n=2 EF optimization criterion, the main poloidal mode number we are interested in is the m=4, which can resonate at the q=2 surface, location of a strong plasma instability [7, 8]. In principle, the m=3 and the m=5 mode numbers should be also investigated in this study but the 3/2 and the 5/2 MHD modes have never been a concern during MAST operation. For this reason, the cancellation of the resonant field at the q=2, both in vacuum and in the presence of plasma, has been reported here.

  Figure 13 shows the resonant n=2 radial magnetic field components as a function of ψ_p in vacuum approximation, in black, and including the response of the plasma, in red. In vacuum approximation, the n=2 resonant magnetic field is small in the plasma core, compared to that near the edge. With the inclusion of the plasma response, the resonant field amplitude is significantly reduced everywhere inside the plasma. This is mainly due to the strong shielding effect coming from the fast

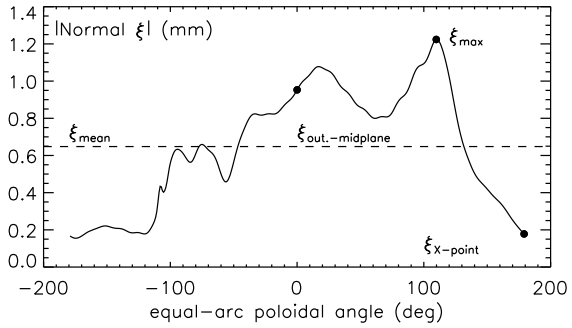

Figure 14: Normal displacement of the plasma surface as a function of the poloidal angle in straigh-line coordinate predicted by the MARS-F code. Different metrics for the minimization of the plasma displacement are also highlighted, i.e. the mean displacement, the maximum displacement, the displacement near the X-point and the outboard midplane displacement.

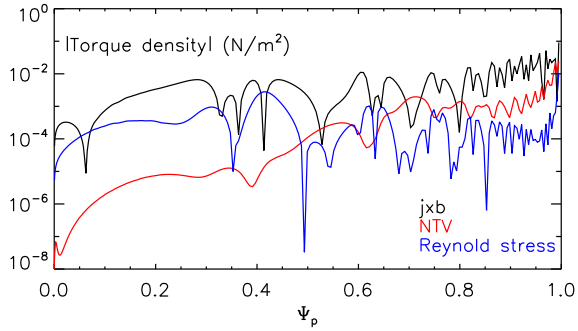

Figure 15: Comparison of various toroidal torques density, i.e. the resonant EM j×b torque (in black), the NTV torque (in red) and the torque due to the Reynold stress (in blue).

toroidal plasma rotation which is about 5% of the Alfvén speed.

- Minimization of the 3D plasma distortion

  Several experiments have shown that the presence of non-axisymmetric magnetic field perturbations can cause a 3D deformation of the plasma boundary [63]. 3D plasma displacement can have detrimental effects on the plasma, such as the triggering of the density pump-out [60–62]. It is thus important to reduce the 3D plasma deformation to the lowest possible amplitude.

  We can define various metrics for this criterion which aim to minimize the 3D plasma distortion, namely the maximum amplitude of the displacement along the poloidal circumference, ξ_{max}, the average amplitude of the displacement, ξ_{mean}, the outboard midplane displacement, $\xi_{out.-midplane}$, and the displacement near the X-point position, $\xi_{X-point}$.

  All these metrics are represented in figure 14, which shows the normal displacement of the plasma surface as a function of the poloidal angle in straight-line coordinate. The displacement is higher around $\theta = 110^o$ because the lower ELM coils row have been used for the n=2 EF control in the plasma modelled. The displacement is also large around $\theta = 0^o$ because of the kink-ballooning.

- Minimization of the net total torque

  In MAST n=2 EF control experiments, a braking of core rotation has been observed. Since the sustainment of plasma rotation is beneficial for the plasma through different mechanisms, such as passive MHD stabilization, magnetic screening effect, turbulence suppression, it is reasonable to consider the minimization of the total torque acting on the plasma as n=2 EF optimization criterion.

  The torques responsible for the rotation braking have been investigated by MARS-F code considering in the momentum balance equation the resonant j×b EM torque, the NTV torque and the Reynolds torque. The j×b torque is associated with shielding currents arising at the resonant surfaces, the NTV results from the toroidal drag force experienced by the plasma particles moving along field lines distorted by the magnetic field perturbations [64, 65], the Reynolds torque is linked to the plasma inertia, the perturbed velocity and the field line stochastization induced by the external magnetic field [66].

  Figure 15 compares the computed radial distributions of the jxb, the NTV and the Reynolds torque densities, considering the plasma response to the combined field, i.e. intrinsic EF + ELM coils.

  MARS-F foresees that the resonant j×b torque plays a major role in the momentum balance equation in the modelled plasma being about one and two order of magnitude larger than the NTV and the Reynolds torques, respectively.

  Since there are several rational surfaces for the n=2 response and the rotation braking is not a localized effect, we have used, as criterion for the n=2 EF correction, the net total torque across all these surfaces. Here the net total torque refers to the total torque integrated across the whole plasma minor radius.

To understand how the various n=2 EF optimization criteria vary changing the ELM coil control parameters and to identify the optimization criteria the best n=2 EF control strategy, experimentally identified, fulfils, MARS-F simulations have been performed scanning the amplitude and the toroidal phase of the external n=2 magnetic field perturbation. In particular, the ELM coil

current has been varied in the range I_{ELM}=[0, 2] kA and the ELM coil phase in the range $\phi_{ELM} = [0^o, 180^o]$.

In the following, examples of MARS-F modelling of various n=2 EF optimization criteria are reported.

Figure 16(a) shows how the resonant magnetic field at q=2, in vacuum approximation, varies changing the ELM coil control parameters. Since such n=2 EF optimization criterion has been also investigated by the ERGOS code to design n=2 EF control experiments, ERGOS and MARS-F predictions can be compared.

MARS-F modelling suggests a minimum of b_{res} at q=2 for I_{ELM}=0.3 kA and $\phi_{ELM} = 120^o$, instead, ERGOS modelling for I_{ELM}=0.5 kA and $\phi_{ELM} = 120^o$. These ELM coil control sets are indicated with a white cross and white star in figure 16(a), respectively.

Note that a good agreement between the codes can be found on the prediction of the optimal ϕ_{ELM}, but a different optimal I_{ELM} is foreseen. The reason of such a discrepancy is due to the fact that unfortunately, a rough I_{ELM} scan has been carried out by the use of the ERGOS code in preparation to n=2 EF control experiments. The I_{ELM} values modelled were $I_{ELM} = [0.5, 1, 1.2]$ kA. During the experimental campaign the time dedicated for n=2 EF control studies did not allow to explore a wide range of I_{ELM}. Only two I_{ELM} values have been tested, i.e. $I_{ELM} = [0.5, 1]$ kA, and the lowest ELM coil current value allowed for the lowest rotation braking.

Conversely, through MARS-F modelling, a detail I_{ELM} scan has been performed which allows us to realize that the best ELM coil control set, identified empirically, does not correspond the true optimal ELM coil control set for the minimization of b_{res} at q=2.

A detail I_{ELM} scan performed after n=2 EF control experiments by the use of ERGOS code confirmed that the use of I_{ELM}=0.3 kA and $\phi_{ELM} = 120^o$ are the optimal ELM coil control parameters for the minimization of b_{res} at q=2, confirming MARS-F prediction. This clarifies the apparent discrepancy on the I_{ELM} prediction among ERGOS and MARS-F codes.

If the n=2 EF optimization criterion for b_{res} at q=2 minimization considers, besides the vacuum, also the response of the plasma, the position of its minimum in the ELM coil control space slightly changes with respect to that one foreseen in vacuum approximation. The position of such a minimum is represented with a white star in figure 16(b). The difference in the position of the minimum in the ELM coil control space is due the fact that the rotation field shielding is taken into account considering the full field. Note that the optimal ELM coil control parameters for the minimization of b_{res} at q=2 in presence of plasma are quite close the ones identified empirically, as shown by comparing the position of the white cross and the white star in figure 16(b), respectively.

Figure 16(c) shows how the X-point displacement varies changing the ELM coil control parameters. The trend is quite similar to that one considering the minimization of the resonant radial magnetic field at q=2 considering the plasma response. Also in this case, the ELM coil control parameters for the minimization of the X-point displacement are close to the ones identified empirically, as shown by comparing the position of the white cross and the white star in figure 16(c), respectively.

Figure 16(d) represents the contour plot of the net total torque in the ELM coil control space. Such torque is mainly associated with the jxb term in the momentum balance equation. The NTV torque and the Reynold stress torque amplitudes, varying the ELM coil control parameters, have in fact negligible amplitude with respect to the jxb one.

MARS-F modelling suggests that the rotation braking depends on the toroidal phase of the external n=2 magnetic field perturbation. This code prediction agrees with the experimental results. Indeed, plasmas which used $\phi_{ELM} \approx 30^o$, as the experiments represented in green and in cyan in figure 11(b), have a larger rotation braking with respect to that ones with $\phi_{ELM} \approx 120^o$, as the plasmas shown in blue and in red. Moreover, MARS-F predicts a larger braking of plasma rotation when I_{ELM}=1 kA is used with any ϕ_{ELM}, instead of I_{ELM}=0.5 kA. This trend is also consistent with the experimental results reported in figure 11(b) which show, for example, that the plasma with I_{ELM}=1 kA and $\phi_{ELM} = 120^o$, plotted in red, experiences a rotation braking stronger than that the braking in the plasma with I_{ELM}=0.5 kA and $\phi_{ELM} = 120^o$, highlighted in blue.

Based on MARS-F simulations, the lowest rotation braking is foreseen when I_{ELM}=0.15 kA and $\phi_{ELM} = 100^o$ are used for n=2 EF control. A white cross has been used in figure 16(d) to highlight the location of this minimum in the ELM coil control space. Actually, these ELM coil control parameters are quite close to that ones of the best ELM coil control set, which is indicated in the same figure with a white star.

Note that the ELM coil control parameters for the minimization of the net total torque are quite similar to the ones foreseen for the minimization of b_{res} at q=2 in presence of plasma. This similarity is due to the fact that the sustainment of plasma rotation, mainly determined by the jxb torque in the momentum balance equation, depends on the minimization of the n=2 magnetic field amplitude.

Beside the optimization criteria just described, the minimization of the mean resonant magnetic field in vacuum approximation and including the full magnetic field, and the minimization of the mean displacement, its maximum value, and the midplane displacement have been also considered in this MARS-F modelling study.

The ELM coil control parameters of all the n=2 EF optimization criteria investigated are summarized in figure 17 with different colors and symbols. In particular, the blue color indicates the ELM coil control parameters which minimize the net total torque, the green color the ELM coil control parameters which reduce the 3D plasma displacement, considering various metrics discussed before, the red and the orange colors the ELM coil control parameters which minimize the resonant magnetic field

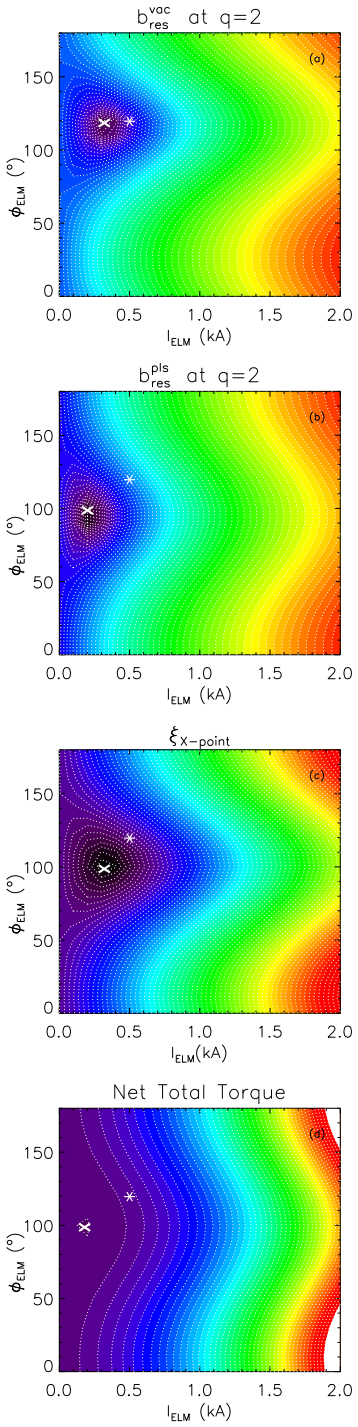

Figure 16: Contour plot of (a) the resonant radial magnetic field at the q=2 magnetic surface in vacuum approximation and (b) including the plasma response, as well, (c) the X-point displacement and (d) the net total torque in the ELM coil control space. The cross indicates the optimal ELM coil control parameters, predicted by the MARS-F code, for each n=2 EF optimization criterion. The star identifies the best ELM coil control parameters for n=2 EF control, experimentally identified.

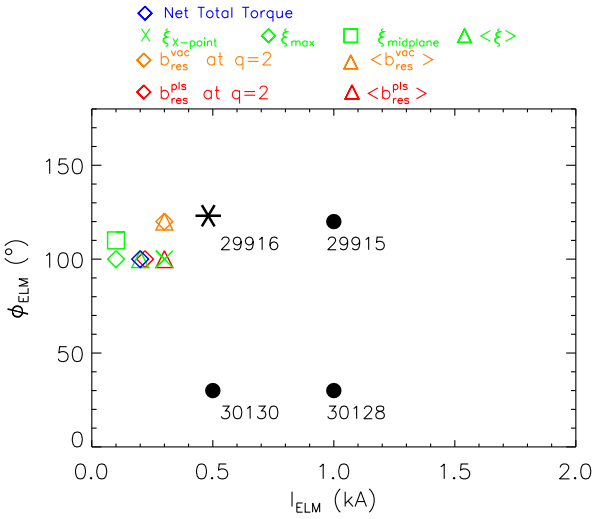

Figure 17: Feedback parameters for n=2 EF control by means of ELM coils as suggested by the MARS-F code for different n=2 EF optimization criteria (different symbols). The dot symbols have been used to indicate the ELM coil control parameters tested in the experiments represented in figure 11, except the best ELM coil control set which is highlighted with a star.

at the q=2 surface and its average value, both in vacuum approximation and by considering also the plasma response, respectively. The symbols are used to indicate different EF minimization metrics within a certain criterion. In the same figure, the ELM coil control parameters used in the experiments presented in figure 11 are reported with black dots, for comparison, except the ELM coil control parameters of the best n=2 EF control set which are indicated with a star.

MARS-F modelling suggests a narrow region in the ELM coil control space which can satisfy the different n=2 EF optimization criteria investigated. Note that, among the ELM coil control sets tested experimentally, the best ELM coil control set is the closest to this narrow region in the ELM coil control space. In particular, among the n=2 optimization criteria, the best n=2 EF control strategy is in better agreement with the minimization of the b_{res} at q=2 in vacuum, which is the criterion that has been investigated through ERGOS modelling to design the n=2 EF control experiments.

Based on MARS-F simulations, by using $I_{ELM} = 0.2 - 0.3$ kA and $\phi_{ELM} = 100^o$ for n=2 EF control, instead of the best ELM coil control set, a minimization of b_{res}, in presence of plasma, both at the q=2 magnetic surface or its mean value, the rotation braking and the plasma displacement, considering different metrics, could be simultaneously achieved.

The fact that similar ELM coil control parameters are foreseen by MARS-F for such different n=2 EF optimization criteria suggests a synergy among them. As a matter of fact, b_{res}, the rotation and the plasma displacement

are linked to each other. The resonant radial magnetic field should be minimized to sustain the rotation being the jxb torque the main responsible for the rotation braking. It is important to sustain the rotation since MARS-F modelling studies, carried out for both MAST and ITER plasmas, have demonstrated that the 3D distortion of the plasma boundary surface is enhanced with decreasing rotation speed [61]. An increase of the 3D distortion of the plasma boundary, especially near the X-point, it is not beneficial for the plasma performance since it can trigger, for example, the density pump-out, as documented in MAST [59] and in other tokamaks [60–62].

By applying the model-based ELM coil control parameters predicted by the MARS-F code, an improvement of the n=2 EF control, and thus of the plasma performance, could be achieved in MAST Upgrade. Note that in the new device, because of 8 ELM coils available in the lower row, instead of the 12 ones in MAST, a toroidal phase shift with 45^o step can be applied. This implies that $\phi_{ELM} = 100^o$ would correspond to an actual toroidal phase of $\phi_{ELM} = 90^o$. To assess the effectiveness of these ELM coil control parameters in improving the n=2 EF control, dedicated experiments have been planned during MAST Upgrade campaign.

It is worth noting that the model-based optimization of the ELM coil control parameters for the n=2 EF control presented here is valid for plasmas in SND configuration. In MAST Upgrade, double null divertor (DND) and upper null divertor (UND) configurations will be investigated, as well. Since in such configurations the ELM coils set employed for n=2 EF control will differ from that one used in SND configuration, ERGOS and MARS-F modelling studies are envisaged to fine-tune the n=2 EF control parameters. Other criteria, such as the overlap criterion proposed in [67], will also be considered in the future to contribute on the identification of the best EF minimization metrics towards ITER operation.

Moreover, this MARS-F modelling on n=2 EF control is based on the assumption that the only source of n=2 EF is the one associated with P4 and P5 coil deformations. Actually, we don't know if other relevant n=2 EF sources are present in MAST Upgrade.

To assess the importance of the n=2 EF amplitude in the new device, the compass scan technique will be used, considering the rotation sustainment as metric. If other n=2 EF sources will be identified, EM modelling will be envisaged and a model-based optimization approach, by the use of ERGOS and MARS-F codes, will be adopted to tune the active control parameters.

V. CONCLUSIONS

This work describes passive and active EF control strategies that have been adopted towards MAST Upgrade operation for minimizing spurious magnetic field perturbations.

Since such perturbations are known to limit the operational space of fusion devices and the plasma performance, in order to guarantee the success of MAST Upgrade, a careful analysis on the intrinsic EF sources in P and D coils has been carried out through high precision magnetic field measurements.

This study is not meant to be an exhaustive overview of all the EF sources, but it is focused on magnetic field errors that can be identified analysing the magnetic field measurements available when writing this manuscript, i.e. the ones associated to D and P coils.

The magnetic field measurements reveal that the main EF harmonics have n=1 and n=2. The approach that has been pursued for controlling these EFs was to compensate them by means of passive control during the construction phase of MAST Upgrade device when possible, instead of using active control during plasma operations.

To this aim, a coil position optimization study has been adopted which allows for the n=1 EF minimization. This is the only EF harmonic that can be compensated by passive control in MAST Upgrade within engineering constrains.

The identification of the optimal coil alignment for the n=1 EF compensation has been obtained by considering high precision magnetic field measurements and corresponding 3D EM modelling. Once identified the movements, i.e. shifts and tilts, that should be applied to each of the P and D coils to guarantee the n=1 EF compensation, such coils have been installed accordingly in the MAST Upgrade device and their alignment has been rigorously checked by photogrammetry.

This passive EF control strategy should minimize the occurrence of plasma terminations associated with EF driven locked modes during MAST Upgrade experiments.

Since a similar level of plasma performance degradation has been observed for n=1 and n=2 magnetic field errors in tokamak devices [46–52], a careful attention on n=2 EF detection and control has been adopted in preparation for MAST Upgrade operation, as well.

The n=2 EF control will be mandatory in the new device since P4 and P5 coil, characterized by a non-negligible n=2 deformation, have been retained in MAST Upgrade from the previous MAST experiment and currents larger than those used in MAST will be used in these coils when exploring high plasma current regimes and various divertor leg configurations.

These aspects have motivated n=2 EF control experiments during MAST operation aiming at characterizing the effect of the n=2 EF on plasma performance and at identifying the optimal n=2 EF active control strategy.

Experiments in which external n=2 magnetic field perturbations have been applied by means of EFCCs have a strong rotation braking. ERGOS modelling reveals that in this case the amplitude of the n=2 EF is increased. This is due to the fact that the EFCCs system, being equipped with 4 coils and 2 power supplies only, cannot induce n=2 magnetic field perturbations with the right phase misalignment for n=2 EF correction.

Promising results on n=2 EF correction have been ob-

tained instead by the use of ELM coils. Being the ELM coils system equipped with various coils and power supplies, it allows more flexibility in fine-tuning the toroidal phase of the external n=2 magnetic field perturbation with the n=2 EF toroidal distribution.

The ERGOS code has been used to guide n=2 EF control experiments by ELM coils, and thus save experimental time. A best ELM coil control set for n=2 EF control have been identified empirically, based on ERGOS predictions, and afterwards MARS-F modelling has been performed to investigate the n=2 EF optimization criteria this best ELM coil control set fulfils.

The MARS-F modelling study identifies a narrow region in the ELM coil control parameter space which fulfils the minimization of different n=2 EF optimization criteria, i.e. the resonant radial magnetic field at the q=2 surface and its mean value, both in vacuum approximation and considering the plasma response as well, the reduction of the net total toque and the plasma displacement considering various metrics.

Notably, the best ELM coil control set, empirically identified, is located closer to this narrow region in the ELM coil control space. This implies that the best n=2 EF control technique, empirically identified, is in agreement not only against the minimization of the resonant radial magnetic field at q=2 in vacuum, as predicted by the ERGOS code, but also against other n=2 EF optimization criteria which include the response of the plasma.

The experience gained on n=2 EF control, from both the experiments and ERGOS and MARS-F modelling, is of fundamental importance for future EF control studies in MAST Upgrade. In particular, the MARS-F modelling suggests a new optimal ELM coil control set for n=2 EF control which takes into account the response of the plasma. By the use of such ELM coil control set, the slightly reduction of the rotation observed in the plasma with the best n=2 EF correction could be reduced. Moreover, a minimization of b_{res}, at q=2 and its mean value, and the plasma displacement considering different metrics could be simultaneously achieved. The effectiveness of such ELM coil control set in reducing the n=2 EF, and thus improving the plasma performance, will be tested in near future EF control experiments in MAST Upgrade.

Based on the experimental and modelling results presented here on n=1 and n=2 EFs control, we can define the multi-n EF control strategies that will be adopted in future MAST Upgrade experiments in SND configuration. The intrinsic n=1 EF associated with P and D coils design and manufacturing process have been reduced by the passive control, i.e. the optimal coil position. The n=2 EF control will deploy the ELM coil system with the optimal control parameters identified by MARS-F modelling.

There is a possible conundrum on this EF control study: besides the n=1 EF associated with P and D coil deformations and the n=2 EF associated with P4 and P5 geometries, we can not exclude a priori the presence in MAST Upgrade of other EFs with non-negligible amplitudes and/or with time-dependent behaviour.

If an n=1 spurious magnetic field error is present, the EFCCs system will be employed for its correction. Similarly, if an n=2 spurious magnetic field error exists, active control by means of ELM coils is envisaged for the compensation of the total n=2 EF amplitude. The multi-n EF active control schemes will use feedforward and/or dynamic current references depending on the static or dynamic EFs nature and ERGOS and MARS-F codes will be exploited to model-based optimize the EF control parameters.

VI. ACKNOLEDGMENT

This work has been carried out within the framework of the EUROfusion Consortium and has received funding from the Euratom research and training programme 2014-2018 under grant agreement No 633053. The views and opinions expressed herein do not necessarily reflect those of the European Commission. This project has also received funding from the RCUK Energy Programme [grant number EP/012450/1]. To obtain further information on the data and models underlying this paper please contact PublicationsManager@ccfe.ac.uk.

[1] Scoville J.T. et al 1991 *Nucl. Fusion* **31** 875
[2] Buttery R.J. and Giruzzi G. 2000 *Plasma Phys. Control. Fusion* **42** B61
[3] Wolfe S.M. et al 2005 *Phys. Plasmas* **12** 056110
[4] Menard J.E. et al 2010 *Nucl. Fusion* **50** 045008
[5] Boozer A.H. 2010 *Fusion Sci. and Technol.* **59** 561
[6] La Haye R.J. et al 1992 *Phys. Fluids B* **4** 2098
[7] Buttery R.J. et al 2012 *Phys. Plasmas* **19** 056111
[8] Fitzpatrick R. et al 1991 *Phys. Plasmas* **3** 664
[9] Zhu W. et al 2006 *Phys. Rev. Lett* **96** 225002
[10] Garofalo A. M. et al 2008 *Phys. Rev. Lett* **101** 195005
[11] Frassinetti L. et al 2015 *Nucl. Fusion* **55** 112003
[12] Lazzaro E. et al 2002 *Phys. Plasmas* **9** 3906
[13] Saibene G. et al 2007 *Nucl. Fusion* **47** 969
[14] Varje J. et al 2016 *Nucl. Fusion* **56** 046014
[15] Garofalo A. et al 2012 *Nucl. Fusion* **42** 1335
[16] Sabbagh A.S. et al 2006 *Nucl. Fusion* **46** 635
[17] Liu Y.Q. et al 2016 *Nucl. Fusion* **56** 066001
[18] Wolfe S.M. et al 2005 *Phys. Plasmas* **12** 056110
[19] MaraschekM. etal 2013 Measurement and impact of the n = 1 intrinsic error field at ASDEX Upgrade 40th EPS Conf. on Plasma Physics (Espoo, Finland, 1?5 July 2013) p P4.127 (http://ocs.ciemat.es/EPS2013PAP/pdf/P4.127.pdf)

[20] Buttery R.J. et al 1999 *Nucl. Fusion* **39** 1827
[21] Luxon J.L. 2002 *Nucl. Fusion* **42** 614
[22] Wang H.Q. et al 2016 *Nucl. Fusion* **56** 0066011
[23] Volpe F.A. et al 2013 emphNucl. Fusion **53** 043018
[24] Shiraki D. et al 2015 *Plasma Phys. Control. Fusion* **57** 025016
[25] In Y. et al 2015 *Nucl. Fusion* **55** 043004
[26] Buttery R.J. et al 2000 *Nucl. Fusion* **40** 807
[27] Howell D. F. et al 2007 *Nucl. Fusion* **47** 1336
[28] Menard J.E. et al 2010 *Nucl. Fusion* **50** 045008
[29] Battaglia D.J. et al 2018 *Nucl. Fusion* **58** 046010
[30] Piron L. et al 2011 *Nucl. Fusion* **63** 063012
[31] Piras F. et al 2010 *Fusion Eng. Design* **85** 739-744
[32] La Haye R.J. et al 1991 *Rev. Sci. Instrum.* **62** 2146
[33] Luxon J.L. et al 2003 *Nucl. Fusion* **43** 1813
[34] Piron L. et al 2011 *Plasma Phys. Control. Fusion* **54** 084004
[35] Kirk A. et al 2014 *Plasma Phys. Control. Fusion* **56** 104003
[36] Liu Y.Q. et al 2014 *Plasma Phys. Control. Fusion* **56** 104002
[37] Morris A. W. et al, "MAST Accomplishments and Upgrade for Fusion Next-Steps" IEEE Transactions on Plasma Science, April 2014
[38] G. Fishpool et al to be submitted
[39] Nardon E. et al 2007 *J. Nucl. Mater.* **363-365** 1071
[40] Liu Y Q et al 2000 *Phys. Plasmas* **7** 3681
[41] Scoville J.T. et al 2003 *Nucl. Fusion* **43** 250
[42] Yang X. et al 2018 *Plasma Phys. Control. Fusion* **60** 055004
[43] Goldston R.J. et al 1981 *J. Comput. Phys.* **43** 61
[44] Lao L.L. et al 2005 *Fusion Sci. Technol.* **48** 968
[45] Foster J. et al, Achieving Tolerable Relative Magnetic Permeability in Austenitic Stainless Steels, 28^{th} SOFT 2014, Symposium on Fusion Technology, San Sebastian, Spain
[46] Lanctot M.J. et al 2017 *Phys. Plasmas* 24 056117
[47] Liang Y. et al 2010 *Nucl. Fusion* **50** 025013
[48] Buttery R.J. et al 2011 *Nucl. Fusion* **51** 073016
[49] Evans T.E. et al 2006 Nat. Phys. 2 419
[50] Unterberg E.A. et al 2010 *Nucl. Fusion* **50** 034011
[51] Lanctot M. J. et al 2013 *Nucl. Fusion* **53** 083019
[52] Kim K. et al 2017 *Nucl. Fusion* **57** 036014
[53] Gerhardt S.P. et al 2010 *Plasma Phys. Control. Fusion* **52** 104003
[54] Paz-Soldan C. et al 2015 *Nucl. Fusion* **55** 083012
[55] Ryan D. A. et al 2015 *Plasma Phys. Control. Fusion* **57** 095008
[56] Ryan D. A. et al 2017 *Plasma Phys. Control. Fusion* **59** 024005
[57] Yang X. et al 2016 *Plasma Phys. Control. Fusion* **58** 114006
[58] Piron L. et al 2010 *Nucl. Fusion* **50** 115011
[59] Kirk A. et al 2011 *Plasma Phys. Control. Fusion* **53** 065011
[60] Evans T. et al 2004 *Phys. Rev. Lett* **92** 235003
[61] Liu Y.Q. et al 2011 *Nucl. Fusion* **51** 083002
[62] Liang Y. et al 2007 *Phys. Rev. Lett* **98** 265004
[63] Callen J.D. 2011 *Nucl. Fusion* **51** 094026
[64] Shaing K. C et al 2010 *Nucl. Fusion* **50** 025022
[65] Park J.K. et al 2007 *Phys. Rev. Lett.* **99** 195003
[66] Rozhansky V. et al 2010 *Nucl. Fusion* **50** 034005
[67] Park J-K et al 2011 *Nucl. Fusion* **51** 023003